Optics Letters

Dynamics of soliton cascades in fiber amplifiers

F. R. Arteaga-Sierra,[1,*] A. Antikainen,[1] and Govind P. Agrawal[1,2]

[1]The Institute of Optics, University of Rochester, Rochester, New York 14627, USA
[2]Laboratory for Laser Energetics, 250 East River Rd., Rochester, New York 14623, USA
*Corresponding author: f.arteaga-sierra@rochester.edu

Received 30 June 2016; revised 12 October 2016; accepted 12 October 2016; posted 13 October 2016 (Doc. ID 269411); published 7 November 2016

We study numerically the formation of cascading solitons when femtosecond optical pulses are launched into a fiber amplifier with less energy than required to form a soliton of equal duration. As the pulse is amplified, cascaded fundamental solitons are created at different distances, without soliton fission, as each fundamental soliton moves outside the gain bandwidth through the Raman-induced spectral shifts. As a result, each input pulse creates multiple, temporally separated, ultrashort pulses of different wavelengths at the amplifier output. The number of pulses depends not only on the total gain of the amplifier but also on the width of the input pulse.

OCIS codes: (060.5530) Pulse propagation and temporal solitons; (060.2320) Fiber optics amplifiers and oscillators.

http://dx.doi.org/10.1364/OL.41.005198

Soliton propagation in erbium-doped fiber amplifiers (EDFAs) was studied in the early 1990s, mainly in the context of telecommunications [1–5]. Recent work has focused on supercontinuum (SC) generation using a single or several cascaded amplifiers [6–9]. In this Letter, we consider a single EDFA and study the evolution of femtosecond pulses launched with energy less than that required to form a fundamental soliton of equal duration. We show that multiple cascaded fundamental solitons are created at different distances within the amplifier. Each of them separates from the main pulse because of the Raman-induced frequency shift (RIFS) that moves them outside the gain bandwidth of the amplifier. Multiple fundamental solitons can also form in passive fibers, but their formation requires either modulation instability (long pulses) or soliton fission (short pulses), and both of these processes lead to simultaneous generation of solitons of different powers and durations [10]. The use of a fiber amplifier allows for the generation of multiple cascaded solitons of nearly the same widths and peak powers, without requiring modulation instability or soliton fission.

To study the evolution of short optical pulses inside an EDFA, we solve numerically the well-known generalized nonlinear Schrödinger equation [10,11]. After adding a frequency-dependent gain term, this equation takes the following form in the frequency domain:

$$\frac{\partial\tilde{A}}{\partial z} - i[\beta(\omega) - \beta(\omega_0) - \beta_1(\omega-\omega_0)]\tilde{A} = \frac{g(\omega)}{2}\tilde{A} + i\gamma(\omega)F\left(A\int_{-\infty}^{+\infty} R(T')|A(z,T-T')|^2 \mathrm{d}T'\right), \quad (1)$$

where $\mathcal{F}$ is the Fourier transform operator, $\tilde{A}(z,\omega) = \mathcal{F}[A(z,t)]$ is the Fourier transform of the complex pulse envelope $A(z,t)$, $\beta(\omega)$ is the propagation constant of the optical mode, $\beta_1 = d\beta/d\omega$ calculated at the carrier frequency ω_0 of the pulse, and $T = t - \beta_1 z$ is the time measured in a frame moving with the input pulse group velocity. The nonlinear effects are included through the parameter $\gamma(\omega)$ and a response function $R(t) = (1-f_R)\delta(t) + f_R h_R(t)$ that includes the Kerr nonlinearity through the Dirac delta function and Raman nonlinearity through the commonly used form of the Raman response function $h_R(T)$ for silica with $f_R = 0.18$ [11]. The frequency-dependent amplifier gain $G(z,\omega) = e^{g(\omega)z}$ is taken to be nearly flat over the amplifier bandwidth Ω and is included using a super-Gaussian profile:

$$G(\omega) = (G_0 - 1)\exp\left[-\left(\frac{(\omega-\omega_0)}{\Omega/2}\right)^4\right] + 1, \quad (2)$$

where G_0 is the maximum gain of the amplifier.

We solve Eq. (1) numerically with the split-step Fourier method [11] for a 20 m long EDFA with its zero-dispersion wavelength (ZDW) at 1490 nm. Its gain spectrum is centered at 1550 nm ($\lambda_0 = 2\pi c/\omega_0 = 1550$ nm) and has a 40 nm gain bandwidth [$\Omega/(2\pi) = 5$ THz], which are common values for EDFAs used in telecommunications. EDFA dispersion is included using $\beta_2 = -5.68\ \mathrm{ps}^2/\mathrm{km}$ and $\beta_3 = 0.13\ \mathrm{ps}^3/\mathrm{km}$ at 1550 nm. The nonlinear parameter has the form $\gamma(\omega) = \gamma_0\omega/\omega_0$, where $\gamma_0 = \gamma(\omega_0) = 2\ \mathrm{W}^{-1}/\mathrm{km}$. The amplitude of the input pulse has the form $A(0,T) = \sqrt{P_0}\,\mathrm{sech}(T/T_0)$ with $T_0 = 50$ fs (full width at half-maximum of about 88 fs). Its peak power P_0 is chosen such that the input soliton order is $N = T_0\sqrt{\gamma_0 P_0/|\beta_2|} = 0.7$, resulting in a peak power of 500 W.

Figure 1 shows the temporal evolution of the 88 fs pulse over 20 m for $G_0 = 1$, 2, and 4 dB/m (normalized with respect to the initial pulse amplitude). For $G_0 = 1$ dB/m, the central part of the input pulse forms a fundamental soliton ($N = 1$)

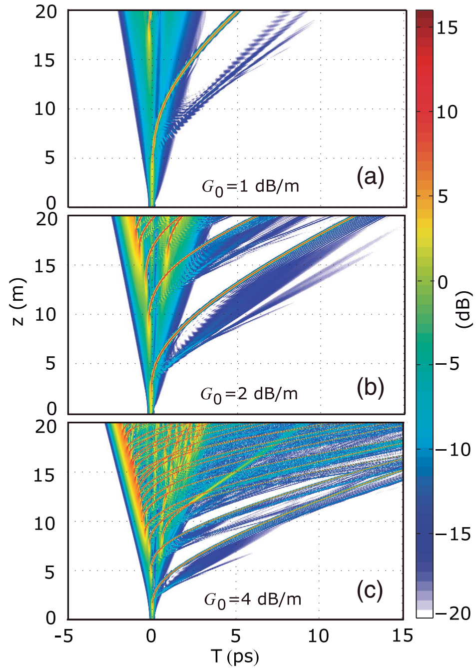

Fig. 1. Temporal evolution of a 88 fs pulse over 20 m of active fiber for (a) $G_0 = 1$, (b) 2, and (c) 4 dB/m. Bent trajectories show redshifted solitons forming at different distances.

after 3 m, and its spectrum begins to redshift because of the RIFS [11], resulting in bending of the soliton trajectory owing to a reduction in its speed relative to the input pulse. The RIFS is relatively large for the soliton because its width is a fraction of the input pulse width. Amplification of this soliton stops after its spectrum moves out of the amplifier bandwidth, but the pulse remnants at $T = 0$ continue to be amplified, as seen in Fig. 1(a). We even see the formation of a second soliton at a distance of about 15 m. Indeed, for a higher gain of $G_0 =$ 2 dB/m in Fig. 1(b) we observe multiple cascaded solitons form at different distances, and their trajectories bend toward the right because of RIFS. Each soliton also sheds some energy in the form of a dispersive wave (DW), as seen in Fig. 1(b). The situation becomes much more complex in Fig. 1(c) where the amplifier gain is increased to 4 dB/m. A large number of cascaded solitons emerge, together with their DWs that travel at different speeds and occasionally collide with the solitons.

One may wonder how the pulse spectrum evolves inside a fiber amplifier and how the input pulse duration affects the evolution. Figure 2 shows the spectral and temporal evolutions for two different input pulse durations for an amplifier with a gain of 3 dB/m. Figures 2(a) and 2(b) clearly show the red shifted spectral bands of the first two solitons formed at distances of about 2 and 6 m. Beyond that several solitons emerge in rapid succession so that their spectra overlap. At the amplifier output, a kind of SC is formed with multiple fundamental solitons and their corresponding DWs. It is noteworthy that, unlike in conventional SC generation, the spectral broadening here is not based on soliton fission because the pulse energy never reaches the level that can support even a second-order soliton. Instead, the spectral broadening is solely due to RIFS, DW generation, soliton collisions, and interactions between DWs and solitons.

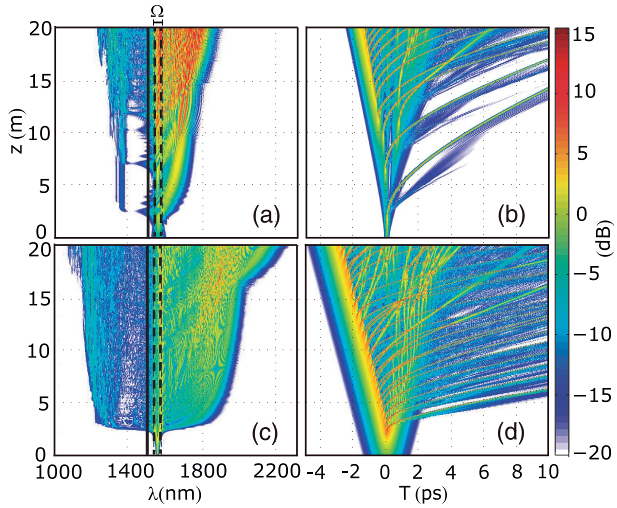

Fig. 2. Spectral [(a) and (c)] and temporal [(b) and (d)] evolution under the conditions of Fig. 1 with $G_0 = 3$ dB/m. The temporal FWHM is 88 fs in [(a) and (b)] and 880 fs in [(c) and (d)]. The ZDW is marked by a black line, and the dashed lines show the gain band. The input soliton order is 0.7 for both cases.

In the extreme, soliton interactions can lead to the generation of abnormally redshifted rogue solitons [12–14]. Figures 2(c) and 2(d) show signs of such a rogue wave being generated after 15 m of propagation. The rogue wave subsequently passes through a train of trailing edge solitons obeying optical Newton's cradle dynamics and gaining more energy from the weaker solitons [15]. The scattering of the previously generated DWs off the moving refractive index barriers associated with the intense rogue solitons then causes the DWs to blueshift further, as seen after 17 m of propagation. Such soliton–DW interactions can also affect the soliton trajectories and therefore mediate solitons collisions [16]. However, such collisions are less common here than in conventional SC generation, which might be beneficial in terms of coherence and control over the evolution dynamics.

The active fiber succeeds in inhibiting soliton collisions because all the leading edge solitons emerge from nearly identical surroundings but at different points in space and time. Because of RIFS, the solitons' group velocities are such that they help preserve the existing temporal gaps. Second, the solitons become surrounded by DWs on both sides, and the effect of one DW on the trajectory of a soliton will be at least partially negated by that of another DW on the other side of the soliton. These effects can be seen in Figs. 1 and 2 where we have numerous solitons with nearly parallel trajectories in a sea of DWs, and soliton collisions occur mostly between leading edge and trailing edge solitons.

It is clear from Figs. 1 and 2 that a single optical pulse propagating inside an optical amplifier can produce a cascade of ultrashort fundamental solitons, whose wavelengths are different at the amplifier output because each soliton forms at a different distance before experiencing RIFS. The dynamics of these solitons exhibit rich behavior because of the simultaneous presence of a DW associated with each soliton and the possibility of collisions between two solitons or between a soliton and a DW. The number of solitons created can be controlled by varying the rate of amplification and the length over which pulse amplification occurs.

As an example, we study the case in which the optical gain exists only over the first few meters, i.e., an active section is followed by a passive fiber section. Figure 3 shows the temporal and spectral evolutions in two cases with $G_0 = 3$ dB/m. The gain is turned off after 2.5 m in the top row but after 7 m in the bottom row. As seen in the figure, only a single soliton forms in the low-gain case. The soliton decelerates even in the passive section and moves slower compared to the pulse remnants because of the RIFS [17]. A DW also appears because of energy transfer from the soliton at a phase-matched frequency during the process of spectral shifting [see parts (a) and (c)]. Since both the DW and the soliton spectra are distinct from the spectrum of input pulse, we can approximately calculate the soliton order by fitting a hyperbolic secant to the pulse remnants. The results are shown in Fig. 3(b), where we see that N exceeds 1 in the active section but drops to well below 1 in the passive section. In contrast, if the gain is kept on for a longer distance [parts (d) to (f)], the remnants continue to be amplified causing a second fundamental soliton to be generated at about 7.5 m, as seen in Figs. 3(d) and 3(f). The corresponding soliton order of the pulse remnants is shown in Fig. 3(e).

The number of fundamental solitons at the amplifier output depends heavily on the total gain G_0 of the amplifier. Figure 4 shows the number of solitons formed at the end of a 20 meter long fiber amplifier (no passive section) as a function of G_0 for two different widths of the input pulse. The solitons were counted manually from the evolution traces such as the ones shown in Fig. 1. In order for a pulse to be counted as a soliton, we required that it had started to separate itself from its surroundings and that its spectrum had begun to redshift. Hence, we interpret Fig. 1(a) as showing only one soliton, as the formation of the other soliton amid the pump remnants is not quite complete yet. Figure 1(b) shows six solitons.

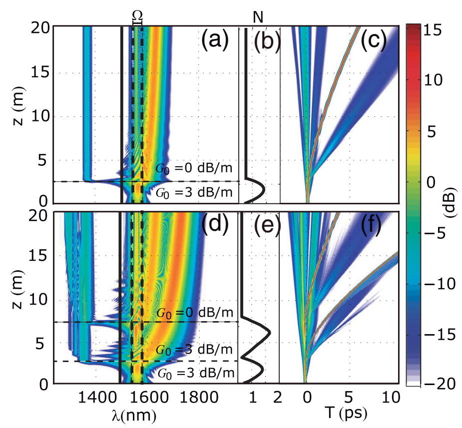

Fig. 3. Spectral [(a) and (d)] and temporal [(c) and (f)] evolution when the fiber is active over 2.5 m (top row) and 7.5 m (bottom row). The soliton order N of the pulse remnants is shown in parts (b) and (e).

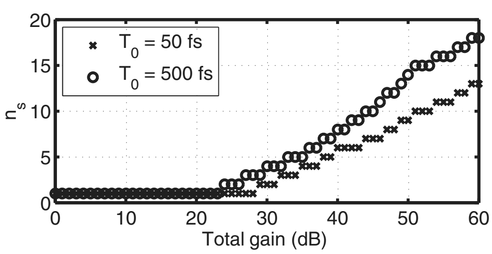

Fig. 4. Number of fundamental solitons (n_s) at the output of a 20 m long amplifier as a function of total gain for two input pulses of different widths launched with $N = 0.7$.

As expected, Fig. 4 shows that the number of solitons at the amplifier output increases with the total gain. For low gains ($G_0 < 22$ dB), a low-energy input pulse forms a soliton within few meters as N approaches 1 and then retains its soliton nature by reshaping itself to become shorter to account for the lack of initial energy. This phenomenon of adiabatic soliton compression is well known [1,5]. It should be stressed that energy for the soliton comes mostly from the central region of the input pulse. After a certain gain threshold that depends on the input pulse duration, the gain is large enough to amplify and reshape the pulse remnants (mostly pulse wings) into another soliton, after the first soliton has moved away because of its slowing down through the RIFS. This process repeats as G_0 is increased, and even more solitons are formed. The leading portion of the input pulse accounts for the formation of most solitons (see Figs. 1 and 2). This is because the RIFS-induced deceleration causes each soliton to lag behind and overlap with the trailing portion. As the solitons slow down, they deplete the trailing edge through nonlinear interactions. As a result, the remaining pulse energy becomes heavily concentrated near the leading edge [see Figs. 2(b) and 2(d)].

Figure 4 shows that the number of solitons n_s at the amplifier output also depends on the width of input pulses. For short pulses ($T_0 = 50$ fs), n_s increases almost linearly with $\ln(G_0)$ or exponentially with G_0. This dependence becomes superlinear (or superexponential) for wider pulses with $T_0 = 500$ fs. One can understand this feature as follows. For wider pulses, the energy is more spread in time. Therefore, it takes a longer distance for a soliton formed near the leading edge of the pulse to reach its trailing edge. If the gain is large enough, the trailing edge of the input pulse can have enough time to create a soliton before it is consumed by the decelerating soliton. By the time the soliton from the leading edge reaches the newly formed trailing edge soliton, their frequency separation is too large for the two solitons to collide and interact nonlinearly. As a result, both solitons survive and separate from the input pulse. The solitons formed in the trailing region of the long input pulse are responsible for the superlinear behavior seen in Fig. 4. The solitons forming in the trailing edge start redshifting and lagging behind, and during this process they gain energy from the nonsolitonic trailing edge pulse remnants through the Raman effect. The trailing edge solitons have a group velocity closer to the pulse remnants and therefore nonlinear interactions between these solitons and the trailing edge pulse remnants take place over longer propagation distances, making the energy transfer to the solitons more efficient. As the trailing edge pulse remnants lose energy to the solitons, there is less energy left to form more solitons through gain, and the growth of the number of solitons with increasing total fiber gain saturates back to linear when the total gain is greater than 50 dB, as can be seen in Fig. 4. The larger number of trailing edge solitons for longer pulses is also evident in the differences between the short pulse temporal evolution shown in Fig. 2(b) and the long pulse evolution shown in Fig. 2(d). Few trailing edge solitons can be seen in Fig. 2(b), whereas they are plentiful in Fig. 2(d) and many of them survive the collisions between leading edge solitons, as can be seen between the 5 and 15 m marks in Fig. 2(d).

The total gain also affects the spectral extent of the output. To study the effect of gain on the output spectrum, we define the spectral range S_r as the difference between the largest and smallest frequencies for which the spectral power is 50 dB below the maximum value. Note that this definition allows for gaps in the spectrum and should not be thought of as the bandwidth of the output spectrum. Figure 5 shows how S_r at different distances of the active fiber depends on the total gain G_0 for the same two different pulse durations used in Fig. 4.

One can identify several different regions in Fig. 5. The spectral range is below 20 THz in the blue region where the pulse evolves to form a fundamental soliton that slowly redshifts through the RIFS. The transition to the teal/green region of Fig. 5(a) indicates the emission of a blueshifted DW that increases S_r to nearly 50 THz (or 400 nm). For example, for 60 dB total gain, the DW is emitted around 2.5 m, as seen in Fig. 2(a). Hence, there is an abrupt change in the spectral range around 2.5 m. When the gain is sufficient, the first soliton continues to be amplified before it leaves the gain window all the way up to the point where it needs to readjust by shedding off a DW. Further propagation gradually extends S_r because the RIFS increases the frequency separation between the DW and the soliton. Indeed, S_r is close to 70 THz in the yellow region in Fig. 5.

For the short-pulse case shown in Fig. 5(a), a second smaller abrupt change occurs when the gain is high enough (red region for $G_0 > 40$ dB). The physical reason for this change is related to reflection of a DW from the moving index boundary created by a decelerating soliton formed later. As is well known, such temporal reflections cause the DW to blueshift further [18,19] and eventually extend the spectral range to beyond 100 THz. This is also visible in Figs. 2(a) and 2(b) where a blueshifted new DW component appears after 15 m. The same physical processes occur in the case of longer pulses shown in Fig. 5(b) with some differences. First, the increase in the spectral extent is more gradual after the first DW generation. It can be attributed to interactions between two or more solitons and between a soliton and a DW, as can be seen in Figs. 2(c) and 2(d). Second, extension to the red side can also happen through the formation of an abnormally redshifted soliton (an example of an optical rogue wave) because of in-phase collisions of solitons [12–14].

In conclusion, it was shown that the amplification leads to a cascade of temporally separated independent solitons of different wavelengths. The cascading process has its origin in RIFS that redshifts the spectrum of solitons while also slowing them down. The associated spectral broadening was attributed to soliton interactions and DW generation. The leading portion of the input pulse was shown to be responsible for the generation of the vast majority of solitons for ultrashort pulses, but the trailing part was also found to generate solitons for wider input pulses. We also found that the number of solitons at the fiber output depends not only on the total gain but also on the width of the input pulse. Even though we focused on an EDFA with a 40 nm gain bandwidth in this work, our results should apply to all fiber amplifiers, as long as the dispersion is anomalous within the gain bandwidth. Our results are interesting from a fundamental perspective but they also point to a potential application. Temporally separated pulses of different wavelengths are often required in practice for applications in areas such as optical coherence tomography [20–22], spectroscopy [23], and multispectral imaging [24]. Moreover, relative delays and wavelengths of different pulses are controllable through the length and gain of the amplifier and the width and peak power of the input pulse.

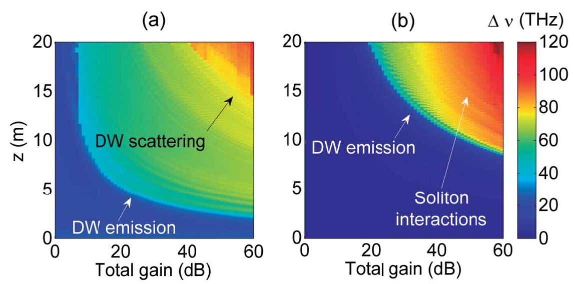

Fig. 5. Spectral range (color coded) as a function of propagation distance and total gain for input pulses with (a) $T_0 = 50$ and (b) 500 fs ($N = 0.7$ in both cases).

Funding. FRAS: Consejo Nacional de Ciencia y Tecnología (CONACYT) (262831); AA: Väisälä Grant of the Finnish Academy of Science and Letters; GPA: National Science Foundation (NSF) (ECCS-1505636).

REFERENCES

1. M. Nakazawa, K. Kurokawa, H. Kubota, K. Suzuki, and Y. Kimura, Appl. Phys. Lett. **57**, 653 (1990).
2. M. Nakazawa, Y. Kimura, and K. Suzuki, IEEE J. Quantum Electron. **26**, 2103 (1990).
3. G. P. Agrawal, IEEE Photon. Technol. Lett. **2**, 875 (1990).
4. G. P. Agrawal, Opt. Lett. **16**, 226 (1991).
5. G. P. Agrawal, Phys. Rev. A **44**, 7493 (1991).
6. P. H. Pioger, V. Couderc, P. Leproux, and P. A. Champert, Opt. Express **15**, 11358 (2007).
7. R. Song, J. Hou, S. Chen, W. Yang, and Q. Lu, Opt. Lett. **37**, 1529 (2012).
8. J. Swiderski and M. Maciejewska, Appl. Phys. B **109**, 177 (2012).
9. M. Tao, T. Yu, Z. Wang, H. Chen, Y. Shen, G. Feng, and X. Ye, Sci. Rep. **6**, 23759 (2016).
10. J. M. Dudley, G. Genty, and S. Coen, Rev. Mod. Phys. **78**, 1135 (2006).
11. G. P. Agrawal, *Nonlinear Fiber Optics*, 5th ed. (Academic, 2013).
12. A. Antikainen, M. Erkintalo, J. M. Dudley, and G. Genty, Nonlinearity **25**, R73 (2012).
13. R. Driben and I. Babushkin, Opt. Lett. **37**, 5157 (2012).
14. J. M. Dudley, F. Dias, M. Erkintalo, and G. Genty, Nat. Photonics **8**, 755 (2014).
15. R. Driben, B. A. Malomed, A. V. Yulin, and D. V. Skryabin, Phys. Rev. A **87**, 063808 (2013).
16. R. Driben, A. V. Yulin, A. Efimov, and B. A. Malomed, Opt. Express **21**, 19091 (2013).
17. N. Akhmediev and A. Ankiewicz, *Solitons: Non-Linear Pulses and Beams* (Chapman & Hall, 1997).
18. A. V. Gorbach and D. V. Skryabin, Phys. Rev. A **76**, 053803 (2007).
19. B. W. Plansinis, W. R. Donaldson, and G. P. Agrawal, Phys. Rev. Lett. **115**, 183901 (2015).
20. P. Cimalla, J. Walther, M. Mehner, M. Cuevas, and E. Koch, Opt. Express **17**, 19486 (2009).
21. F. R. Arteaga-Sierra, C. Milián, I. Torres-Gómez, M. Torres-Cisneros, A. Ferrando, and A. Dávila, Opt. Express **22**, 2451 (2014).
22. F. R. Arteaga-Sierra, C. Milian, I. Torres-Gómez, M. Torres-Cisneros, G. Moltó, and A. Ferrando, Opt. Express **22**, 23686 (2014).
23. E. Lareau, F. Lesage, P. Pouliot, D. Nguyen, J. Le Lan, and M. Sawan, J. Biomed. Opt. **16**, 096014 (2011).
24. Q. Cao, N. G. Zhegalova, S. T. Wang, W. J. Akers, and M. Y. Berezin, J. Biomed. Opt. **18**, 101318 (2013).